Interdisciplinary Research in Medical Sciences Specialty
ISSN: 3062-4401
2026, Volume 6, Issue 1, Page No: 145-163
Copyright CC BY-NC-SA 4.0
Available online at: www.galaxypub.co/page/journals

Galaxy Publication

Single-Cell Pan-Cancer Analysis Reveals MEG3 Dysregulation in Cancer-Associated Fibroblasts and Its Role in CAF Subtype Specification

Gabriel Costa[1]*, Lucas Ribeiro[1], Ricardo Alves[2], Mariana Lopes[3]

[1]Department of Pan-Cancer Genomics and Single-Cell Analysis, Faculty of Medicine, Federal University of Minas Gerais, Belo Horizonte, Brazil.
[2]Department of Cancer-Associated Fibroblasts and Long Non-Coding RNA, Faculty of Medicine, University of Coimbra, Coimbra, Portugal.
[3]Department of CAF Subtype Specification, Faculty of Medicine, University of São Paulo, São Paulo, Brazil.

***E-mail** ✉ gabriel.costa@ufmg.br

Received: 10 January 2026; **Revised:** 06 April 2026; **Accepted:** 12 April 2026

ABSTRACT

Long non-coding RNAs (lncRNAs) exert essential regulatory effects on the activation and phenotypic conversion of cancer-associated fibroblasts (CAFs). Nevertheless, their involvement has yet to be thoroughly explored using single-cell approaches. Leveraging comprehensive integrated single-cell transcriptomic datasets, we identified lncRNAs with abnormal expression patterns specifically within CAFs, the primary cellular element of the tumor microenvironment. Our analysis uncovered a pan-cancer pattern of pronounced CAF-restricted reduction in Maternally Expressed Gene 3 (MEG3) levels, together with a rise in the fraction of MEG3-positive cells. This alteration appears linked to m6A-dependent post-transcriptional control mechanisms. Pseudotime trajectory reconstruction across key CAF subpopulations revealed that higher MEG3 expression upregulates PDGFRA, which in turn facilitates CAF activation and their shift toward a MEG3-positive adipogenic CAF (MACAF) state. This MACAF subpopulation displays enhanced vulnerability to Dasatinib. Intercellular communication networks associated with MACAFs indicated that these cells stimulate epithelial-mesenchymal transition in cancer cells through TGF-β signaling, thereby increasing tumor cell motility and supporting tumor advancement and invasive behavior. Furthermore, individuals exhibiting higher MACAF scores demonstrated significantly worse survival outcomes and diminished efficacy of immune checkpoint blockade therapy, pointing to a role for MACAFs in establishing an immunosuppressive milieu. Collectively, this work elucidates the contribution of MEG3 to CAF activation and emphasizes the clinical relevance of the MACAF score as a potential biomarker for optimizing treatment regimens that incorporate Dasatinib alongside immunotherapy.

Keywords: Cancer-associated fibroblast, Dasatinib, Immunotherapy, lncRNA, MEG3, PDGFRA

How to Cite This Article: Costa G, Ribeiro L, Alves R, Lopes M. Single-Cell Pan-Cancer Analysis Reveals MEG3 Dysregulation in Cancer-Associated Fibroblasts and Its Role in CAF Subtype Specification. Interdiscip Res Med Sci Spec. 2026;6(1):145-63. https://doi.org/10.51847/vZJvOETNNd

Introduction

The sustained expansion and advancement of cancer cells are strongly dependent on the supportive infrastructure provided by the tumor microenvironment (TME) [1]. Investigations at single-cell resolution have underscored the extensive heterogeneity, adaptive plasticity, and substantial influence of TME features on therapeutic efficacy and patient prognosis in diverse malignancies [2-6]. As tumors evolve, the modified microenvironment attracts various cell lineages, including immune cells, cancer-associated fibroblasts (CAFs), and endothelial cells. In conjunction with the surrounding extracellular matrix (ECM), these elements generate a supportive niche that facilitates tumor cell survival, proliferation, and distant spread [7]. Single-cell studies have thoroughly mapped the evolving and multifaceted changes occurring in the TME throughout tumor development [8-10]. Furthermore, notable differences have emerged in the crosstalk among stromal cells, the ECM, and neighboring cell populations according to tumor histology, molecular traits, disease stage, and individual patient characteristics [11]. In

© 2026 Interdisciplinary Research in Medical Sciences Specialty

particular, the diversity of stromal cell populations and matrix elements is now recognized as a major factor influencing tumor growth, metastatic dissemination, and evasion of immune responses [12, 13]. Therefore, detailed characterization of the dynamic relationships between intracellular processes and extracellular components within tumor stroma is indispensable for formulating effective cancer treatment strategies.

CAFs represent one of the most prominent stromal cell types in the TME and are typically characterized by persistent aberrant activation, which helps establish a disease-promoting microenvironment [14]. Their remarkable plasticity and functional diversity within the changing TME play pivotal roles in driving tumor progression and conferring resistance to immunotherapeutic interventions [2, 15]. The complex network of intercellular signals exchanged between CAFs and other TME residents can govern processes such as neovascularization, ECM reorganization, and resistance to immune checkpoint blockade, ultimately fostering tumor expansion and adverse clinical outcomes [16]. Moreover, continuous reciprocal interactions between CAFs and neoplastic cells help sustain the activated phenotype of CAFs. Signaling cascades involving pathways such as TGF-β, NOTCH, and CXCL12, among others, enhance tumor cell proliferation, motility, and invasive capacity, thereby promoting metastasis and therapeutic refractoriness [17]. In parallel, epithelial and endothelial cells have been proposed as possible origins of CAFs through processes including epithelial-mesenchymal transition (EMT) and endothelial-mesenchymal transition [2, 18-20]. Additionally, these cells can trigger the conversion of normal fibroblasts (NFs) into CAFs by releasing cytokines such as FGF and PDGF, along with corresponding receptor-ligand engagements [14, 21].

The advent of single-cell RNA sequencing (scRNA-seq) and spatial transcriptomics has enabled refined classification of CAF subpopulations and improved understanding of their varied developmental origins and activation pathways [2, 22-24]. Distinct CAF subsets have been demonstrated to establish an immunosuppressive milieu through targeted cellular interactions and the production of multiple soluble mediators, assisting cancer cells in avoiding immune recognition [2, 25, 26]. These subpopulations are also acknowledged for their capacity to modulate responses to immune checkpoint inhibitors [23-25, 27]. Targeted approaches against specific CAF subsets are actively being explored, indicating an expanding appreciation of their relevance in cancer pathobiology. Despite these advances, the precise regulatory mechanisms and critical molecular drivers underlying CAF activation and lineage conversion remain largely elusive. Important gaps persist in our knowledge of how individual CAF subtypes influence tumor evolution and immune evasion. Resolving the molecular hallmarks of the NF-to-CAF transition and pinpointing reliable CAF-restricted markers will deepen our insight into cancer pathogenesis and facilitate improvements in early diagnosis and treatment.

Long non-coding RNAs (lncRNAs) constitute a significant group of non-protein-coding transcripts that orchestrate multifaceted communication between the TME and malignant cells, positioning them as valuable candidates for diagnostic and therapeutic applications [28, 29]. Comparative high-throughput sequencing analyses have revealed pronounced differences in lncRNA expression profiles between CAFs and NFs [30, 31]. Several lncRNAs preferentially expressed in CAFs have been linked to enhanced tumor cell proliferation, metastatic behavior, and resistance to cytotoxic therapies [32-34]. Clarifying the functional contributions of lncRNAs to CAF-cancer cell interactions holds considerable potential for uncovering new biomarkers and designing innovative anticancer strategies. Although lncRNAs have been profiled via scRNA-seq in tumor-associated T lymphocytes [35], a systematic single-cell resolution examination of CAF-specific lncRNAs has not yet been performed.

In the current investigation, we employed extensive pan-cancer scRNA-seq datasets to delineate the distinctive molecular attributes of CAFs compared with NFs. This analysis uncovered a selective downregulation of the lncRNA Maternally Expressed Gene 3 (MEG3) in CAFs, likely regulated by m6A modifications. Such downregulation appears to stimulate CAF activation and drive their differentiation toward an adipogenic CAF (adiCAF) subpopulation in the TME, identifying a candidate therapeutic vulnerability and a potential indicator of immunotherapy responsiveness. Overall, this work provides a foundation for future studies on the contributions of MEG3 within the TME and supports the development of the MACAF score as a biomarker to inform novel therapeutic strategies in oncology.

Materials and Methods

Single-cell RNA-seq data preprocessing and quality control

All raw single-cell RNA sequencing data were processed using the `cellranger count` pipeline implemented in Cell Ranger software (version 6.1.2). Reads were aligned and quantified against the GRCh38 human reference genome. The resulting output matrices generated by Cell Ranger were subsequently imported into the Seurat R package (version 4.3.0.1) for downstream quality control and analysis.

Data integration and quality filtering

Individual sample datasets were first loaded and converted into Seurat objects via the `Read10X` function. These objects were then merged into a unified dataset using the `merge` function. Rigorous quality control thresholds were applied to exclude low-quality cells and genes. Retained cells were required to express more than 200 genes while exhibiting less than 20% mitochondrial gene content. Genes were retained only if expressed in at least three cells. Additionally, cells with fewer than 200 or more than 6000 detected genes were removed to further eliminate potentially compromised cells.

Doublet identification and exclusion

Potential doublets were detected and removed using the DoubletFinder algorithm with default parameters. Following this filtering process, the final cleaned dataset comprised 675,208 high-quality cells, encompassing both malignant and non-malignant populations from unsorted specimens.

Normalization and variable feature selection

Data normalization was performed using the “LogNormalize” method with a scale factor of 10,000 to account for variations in sequencing depth across individual cells. The top 2000 most variable genes were then identified, as these capture biologically relevant variation more effectively than technical artifacts. The influence of mitochondrial gene percentage was regressed out from the normalized expression matrix using the `ScaleData` function, in accordance with standard Seurat workflows.

Dimensionality reduction and batch effect correction

Principal component analysis (PCA) was conducted for dimensionality reduction, retaining the top 30 principal components based on feature standard deviations. Unsupervised clustering was performed using the `FindNeighbors` and `FindClusters` functions. Visualization of the resulting clusters was achieved through Uniform Manifold Approximation and Projection (UMAP). To mitigate batch effects arising from patient-specific differences across datasets, the `RunFastMNN` function (default parameters) from the SeuratWrappers package (version 0.3.1) was applied to harmonize expression profiles.

Cell type annotation

Cell populations were annotated according to the expression of well-established lineage-specific marker genes. Following initial clustering, differentially expressed genes (DEGs) were identified for all clusters using the `FindAllMarkers` function in Seurat at a resolution of 2.0. Annotation was performed by cross-referencing cluster-specific expression patterns with canonical markers: Endothelium (VWF, RAMP2, PECAM1, CLDN5, PLVAP), Epithelium (EPCAM, KRT18, KRT19, REG1B), Fibroblasts (LUM, DCN, FBN1, COL1A1, COL1A2), Lymphocyte (CD2, CD3D, CD3E, NKG7, IL7R, PTPRC), Myeloid (TYROBP, CD68, LYZ, MS4A2, TPSB2), and Plasma (IGHG1, IGKC, IGLC2, JCHAIN).

To resolve heterogeneity within the fibroblast compartment, a dedicated round of dimensionality reduction and clustering was performed exclusively on fibroblast cells at a resolution of 1.2. Subtype annotation was based on distinctive marker genes differentially expressed within these subclusters, as detailed in the accompanying figures.

Trajectory inference for CAF subpopulations

To reconstruct the activation trajectory of CAFs, pseudotime analysis was conducted on the fibroblast population. A random subset of 30,000 fibroblast cells was selected for this analysis using Monocle 2 (version 2.26.0). Monocle objects were generated from the expression matrix via the `NewCellDataSet` function. Size factors and dispersions were estimated to normalize for differences in mRNA capture efficiency across cells. Following normalization, genes exhibiting differential expression across developmental states were identified and used to order cells along a trajectory. This approach enabled the delineation of progressive activation states within the

fibroblast population in the tumor microenvironment. The resulting trajectory was annotated and visualized to illustrate transitions among CAF subpopulations and their contributions to cancer progression.

Cell–cell interaction analysis

To systematically characterize intercellular communication networks within the tumor microenvironment (TME), analyses were conducted using the CellChat package (version 1.6.1). Particular emphasis was placed on assessing the impact of MEG3 expression on these interactions. Input data were partitioned according to MEG3 status, generating two distinct groups: MEG3-positive and MEG3-negative cells. This stratification permitted direct comparison of communication profiles between the two populations. Interaction strengths and networks among various cell types were quantified and evaluated within each group using CellChat. This strategy enabled the detection of statistically meaningful differences in cell-cell signaling attributable to MEG3 expression. Built-in visualization tools within CellChat were utilized to highlight significant alterations in interaction patterns between the groups. Ligand-receptor pairs reaching statistical significance ($p < 0.05$) were extracted for quantitative analysis and graphical representation.

NicheNet analysis

NicheNet modeling was executed with the nichenetr R package (version 2.1.0) to examine signaling from the MACAF subtype to epithelial cells. The MACAF subpopulation was designated as the sender cell type, while all epithelial cells served as receivers. The EMT gene signature was specified as the target gene set to evaluate how MACAF-derived signals might promote EMT in epithelial cells. Potential ligands were defined as those expressed in sender cells with corresponding receptors present in receiver cells. The complete set of genes expressed in epithelial cells constituted the background gene list. Ligand activity was predicted using the `predict_ligand_activities` function, yielding a ranked list of active ligands from the sender population. Ligands were ordered according to the area under the precision-recall curve (AUPR) measuring agreement between predicted targets and observed transcriptional changes. The top 30 ranked ligands and their associated targets were selected for subsequent visualization.

Construction of stable low-expression cell lines

Stable MEG3 knockdown cell lines were established in human colorectal carcinoma-derived fibroblasts (CAF1 and CAF2) and the mouse NIH3T3 fibroblast line through lentiviral transduction. One day prior to infection, cells were plated at equal densities in six-well plates. When cells reached approximately 50% confluence the following day, the culture medium was replaced with 1.5 ml of fresh, pre-warmed complete medium per well. Viral stocks stored at −80°C were thawed on ice, and 500 μL of viral suspension was added to each well together with 1.6 μL of 10 mg/ml polybrene. The plates were gently agitated to ensure uniform distribution and then returned to a 37°C incubator with 5% CO_2. After 16–18 hours, the medium was replaced with 2 ml of fresh complete medium. Knockdown efficiency was verified by real-time quantitative PCR (qPCR). The shRNA sequences targeting human and mouse MEG3, along with the qPCR primer sequences.

Transwell assay

For migration assays, cells were harvested by enzymatic digestion, centrifuged at 800 rpm for 3 min, and washed three times with saline. The cell pellets were resuspended in serum-free medium and enumerated. Cell culture inserts (Transparent PET Membrane, 24-well format, 8 μm pore size; Corning) were placed in 24-well plates containing conditioned medium derived from supernatants of shRNA-treated CAF1, CAF2, and NIH3T3 cultures, with 800 μL of serum-containing medium added to each lower chamber. Then, 200 μL of cell suspension was seeded into the inserts at the following densities: 300,000 cells for RKO, 500,000 cells for HCT116, 50,000 cells for MC38, and 30,000 cells for CT26. CAF-conditioned media were collected every three days and centrifuged at 1600 rpm for 10 min prior to use. Plates were incubated under standard conditions for 24 hours. Following incubation, inserts were removed, and non-migrated cells on the upper membrane surface were gently removed with a cotton swab. Inserts were fixed in paraformaldehyde for 20 min, stained with 1% crystal violet for 20 min, rinsed with water, and air-dried. Representative fields were imaged under a microscope, and migrated cell areas were quantified using ImageJ software.

Transcription factor inference with SCENIC

Gene regulatory network analysis of single-cell transcriptomes was performed using SCENIC software (version 0.12.1) to compare transcription factor (TF) activity between MEG3-positive and MEG3-negative groups. The analysis followed a three-step workflow: (1) co-expression modules between TFs and potential target genes were inferred using GENIE3/GRNBoost; (2) regulons within each module were identified with RcisTarget; and (3) regulon activity was scored across cells using the AUCell algorithm.

Cancer-associated fibroblast subtype signature scoring

Signature gene sets for each fibroblast subtype were defined as the top 25 marker genes identified via the `FindMarkers` function and refined by manual curation. Gene set variation analysis (GSVA) was applied to deconvolute the relative proportions of each fibroblast subtype within pan-cancer bulk RNA-seq expression profiles.

Enrichment and gene set variation analysis

Differential gene set enrichment analysis between groups was conducted using the ClusterProfiler package (version 4.8.1). Pathway activity scores were computed via the GSVA package (version 1.48.2) under non-parametric, unsupervised settings. The Hallmark gene sets (v7.5.1) were retrieved from the Molecular Signatures Database (MSigDB) for all enrichment analyses.

Potential therapeutic drug prediction

Drug sensitivity data and molecular profiles of cancer cell lines were obtained from the CTRP and PRISM pharmacogenomic databases. Following the approach described by Chen Yang *et al*. [36], compounds with more than 20% missing values were excluded, and remaining missing values were imputed using the k-nearest neighbors algorithm. After preprocessing, the drug area-under-the-curve (AUC) matrix and CCLE cell line expression data were used to train a ridge regression model for drug response prediction. This model was then applied to estimate drug sensitivity for clinical samples based on their pan-cancer bulk expression profiles. Candidate drugs were selected according to the criteria of logFC of AUC > 0.1 and Spearman correlation coefficient < −0.2.

Survival analysis

The prognostic significance of selected genes was assessed through univariate Cox proportional hazards regression using continuous expression values, incorporating matched clinical data and transcriptomic profiles obtained from UCSC Xena. Optimal cutoff thresholds for stratification were determined with the `surv_cutpoint` function. Survival probabilities were estimated using the Kaplan-Meier method, and hazard ratios were calculated accordingly. Survival curves were generated via the Kaplan-Meier estimator and visualized using the "survminer" R package (version 0.4.9). Differences in survival between groups were evaluated using the log-rank test implemented in the "survival" R package (version 3.5.5).

TIDE analysis

To determine whether the MACAF signature is associated with tumor immune evasion, Tumor Immune Dysfunction and Exclusion (TIDE) analysis was performed. This computational framework predicts potential responses to immune checkpoint blockade (ICB) therapy based on tumor gene expression patterns. Bulk RNA-seq data from the TCGA pan-cancer cohort were first normalized and subjected to quality filtering. The processed expression profiles were then submitted to the TIDE web portal (http://tide.dfci.harvard.edu). The algorithm evaluates two key mechanisms of immune escape: T-cell dysfunction, observed in tumors containing abundant cytotoxic T lymphocytes yet exhibiting impaired effector function, and T-cell exclusion, in which T cells infiltrate the tumor but fail to penetrate the tumor core. For each sample, the TIDE tool computed an overall TIDE score as well as separate dysfunction and exclusion scores. Lower TIDE scores indicate a greater predicted likelihood of clinical benefit from immune checkpoint inhibitor therapy.

Results and Discussion

Fibroblast-restricted expression pattern of MEG3 at single-cell resolution

To comprehensively examine the functions of lncRNAs within CAFs, we utilized a previously compiled integrated single-cell dataset comprising 226 tumor, adjacent, and normal specimens collected from 164 individuals across 10 prevalent solid tumor types **(Figure 1a)** [2]. After stringent quality filtering and correction for batch effects, a total of 675,208 high-quality cells were retained. Unsupervised clustering combined with established marker gene annotation allowed the identification of seven primary cell lineages **(Figures 1b and 1c)**, encompassing endothelial cells, epithelial cells, fibroblasts, lymphocytes, myeloid cells, and plasma cells. Focusing on the regulatory significance of lncRNAs in oncology, we evaluated lncRNA expression profiles in fibroblasts derived from tumor versus normal tissues for each cancer type. This analysis identified 10 differentially expressed lncRNAs in CAFs that were also detected as altered in the corresponding bulk RNA-seq data from The Cancer Genome Atlas (TCGA) **(Figure 1a)**. Among these candidates, MEG3 exhibited particularly pronounced expression differences in several tumor types **(Figure 1a)**. Prior research has indicated that MEG3 possesses tumor-suppressive properties in malignant cells, partly by modulating key tumor suppressor genes and oncogenes such as p53, RB1, myc, and TGF-β [37-39]. Although present at moderate levels in epithelial cells, MEG3 demonstrates markedly higher prevalence in fibroblasts relative to other cell populations in terms of positive cell fraction, irrespective of tissue malignancy status. A parallel pattern was evident when comparing expression intensity among MEG3-positive cells across lineages **(Figures 1d–1f)**. Notably, MEG3 levels in fibroblasts were substantially reduced in tumor tissues compared with both normal and adjacent non-malignant tissues **(Figure 1g)**. This observation aligns with pairwise differential expression analyses performed on bulk TCGA transcriptomes across multiple cancers. Interestingly, the proportion of MEG3-positive cells was lower in normal samples than in adjacent or primary tumor samples **(Figure 1h)**. This discrepancy may account for the inability to detect reduced MEG3 expression in certain malignancies (e.g., lung cancer) when relying solely on bulk transcriptome data. Validation using independent single-cell cohorts (STAD and CORE) confirmed the consistent expression dynamics of MEG3, thereby strengthening the robustness of these observations. To determine whether this pattern is shared by other tumor suppressor genes, comparable trends were noted for TP53 and CDKN1A, suggesting that tumor suppressor transcripts may display analogous single-cell expression behaviors in neoplastic tissues.

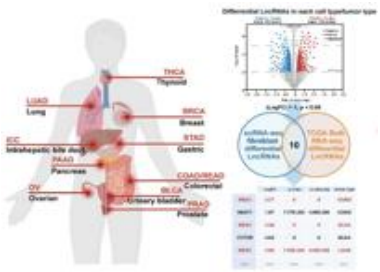

a)

b)

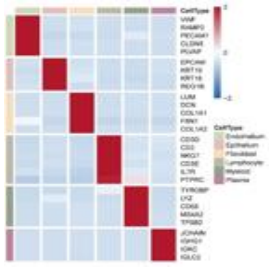

c)

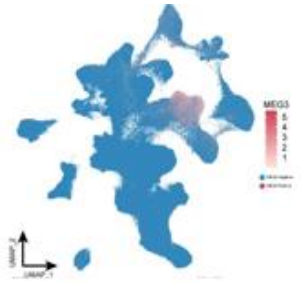

d)

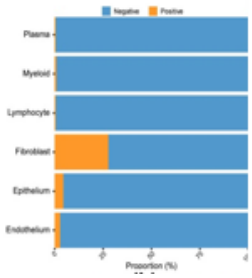

e)

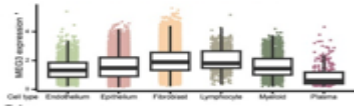

f)

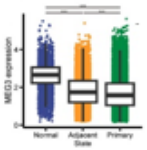

g)

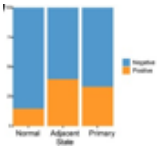

h)

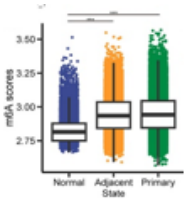

i)

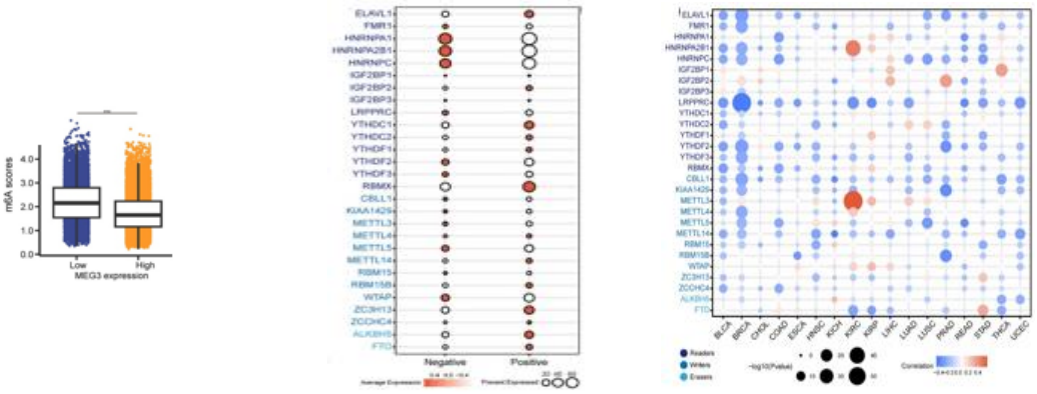

j) k) l)

Figure 1. Pan-cancer single-cell transcriptomic analysis reveals reduced MEG3 expression in cancer-associated fibroblasts.

(a) Overview of the analytical pipeline used to identify MEG3 across pan-cancer single-cell datasets. Differential expression analysis was first conducted separately at the single-cell RNA-seq and TCGA bulk RNA-seq levels, followed by intersection of fibroblast-derived lncRNA candidates. (b) UMAP visualization of 675,208 single cells labeled according to major cell lineages. (c) Heatmap depicting marker gene expression for the principal cell populations. (d) Distribution of MEG3 expression across major cell lineages. (e) Relative proportions of MEG3-positive and MEG3-negative cells within major cell lineages. (f) Boxplot illustrating MEG3 expression intensity in individual cell types. Boxplots display median, interquartile range, and whiskers representing minimum and maximum values, with individual points corresponding to single cells. (g) Differential MEG3 expression according to tissue malignancy status. (h) Proportions of MEG3-positive and MEG3-negative cells stratified by malignant status. (i) Boxplot of m6A pathway activity scores across different tissue states. (j) Boxplot of m6A pathway activity scores in cells with high versus low MEG3 expression. (k) Bubble plot depicting differential expression of m6A-associated genes between MEG3-positive and MEG3-negative cells. (l) Pearson correlation analysis between m6A-related gene transcripts and MEG3 expression. Correlations for MEG3-positive and MEG3-negative cells are shown in red and blue, respectively. Statistical significance was determined using the two-sided Mann–Whitney test. *p < .05, **p < .01, ***p < .001.

The contrasting patterns observed between MEG3 expression levels and the proportion of MEG3-positive cells in tumor versus normal tissues point toward the contribution of post-transcriptional regulatory processes. Since m6A modification represents a predominant mechanism governing lncRNA stability and processing in tumor cells [40], we examined the relationship between m6A pathway activity and MEG3 abundance. Notably, m6A pathway scores exhibited a progressive increase from normal to adjacent to tumor tissues, and were elevated in cells displaying low MEG3 expression **(Figures 1i and 1j)**. Furthermore, MEG3-positive and MEG3-negative populations displayed divergent m6A regulatory signatures at single-cell resolution **(Figure 1k)**, indicating that transcriptional induction of MEG3 coincides with alterations in post-transcriptional control. Supporting evidence from TCGA data revealed a significant negative association between MEG3 transcript levels and m6A-related gene expression across cancers **(Figure 1l)**. Together, these results suggest that m6A-mediated post-transcriptional regulation links CAF activation status with MEG3 expression, thereby reconciling the apparently paradoxical increase in MEG3-positive cell fraction alongside reduced overall MEG3 levels in malignant tissues relative to normal counterparts.

MEG3 transcriptional upregulation across fibroblast subpopulations

Given the preferential expression of MEG3 in fibroblasts, we next examined the transcriptional characteristics of distinct fibroblast subpopulations in greater detail. Re-clustering based on well-established marker genes identified seven fibroblast subtypes **(Figures 2a and 2b)**. Of these, subtype C1 was predominantly composed of cells from normal tissues and was therefore designated as normal fibroblasts (NFs). The remaining subtypes were largely derived from adjacent and tumor samples and were collectively classified as CAFs **(Figure 2c)**. Subtype C4, which displayed the highest fraction of MEG3-positive cells, corresponded to adipogenic CAFs (adiCAF) and exhibited enriched adipogenic pathway activity along with elevated expression of associated markers such as

CFD, PTGDS, and FBLN1. In contrast, subtype C2, showing the lowest MEG3-positive rate, was identified as myofibroblasts (myCAF) **(Figures 2b–2e)**. In line with earlier observations, MEG3 reached its highest expression levels in the C1 (NF) subpopulation, which originates mainly from non-malignant tissues **(Figure 2f)**. Owing to the limited cell counts in subtypes C5–C7 **(Figure 2c)**, subsequent analyses concentrated on the predominant fibroblast clusters. Pseudotime trajectory modeling of CAF activation identified three discrete cellular states **(Figure 2g)**. Two separate differentiation routes emerged from State 1 (enriched for C1/NF cells) leading toward either State 2 (enriched for C2/myCAF cells) or State 3 (enriched for C3 and C4 cells) **(Figures 2h and 2i)**. Along these trajectories, overall MEG3 expression declined while the proportion of MEG3-positive cells increased **(Figures 2j–2k)**. Consistent with these patterns, the NF subpopulation (C1) displayed elevated MEG3 transcript abundance coupled with reduced m6A pathway activity relative to CAF subtypes. Analogous trends were observed when examining the pseudotime trajectories and cellular states of the major CAF populations **(Figures 2l–2n)**.

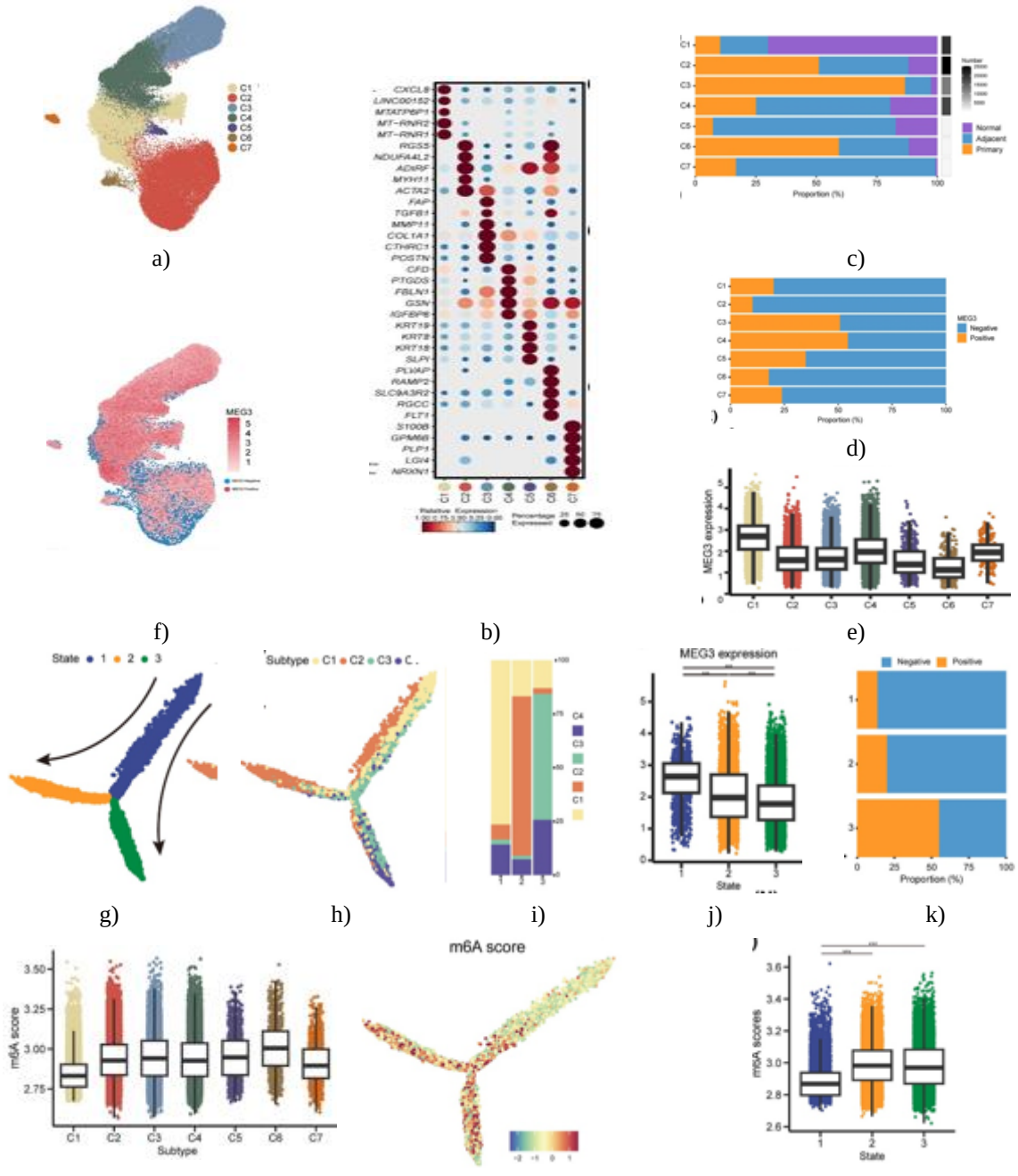

Figure 2. Transcriptional activation of MEG3 across fibroblast subpopulations.

(a) UMAP visualization of fibroblast subtypes identified using established cancer-associated fibroblast marker genes. (b) Dot plot illustrating expression levels of representative marker genes for the primary fibroblast subtypes. (c) Left panel: bar graph depicting the proportional distribution of each fibroblast subtype across normal, adjacent, and tumor tissues. Right panel: heatmap indicating the absolute cell counts for each fibroblast subtype. (d) Proportions of MEG3-positive and MEG3-negative cells within individual fibroblast subtypes. (e) Boxplot comparing MEG3 expression intensity across fibroblast subtypes. Boxplots show the median, interquartile range, and whiskers extending to minimum and maximum values, with individual points representing single cells. (f) Distribution of MEG3 expression levels among fibroblast subtypes. (g) Pseudotime trajectory plot depicting the three defined states within the major CAF populations. (h) Pseudotime trajectory showing the distribution of different CAF subtypes across the three cellular states. (i) Right panel: histogram illustrating the proportional composition of major CAF subtypes within each defined state. (j) Boxplot of MEG3 expression levels across the three CAF states. Boxplots display median, quartiles, and minimum/maximum values, with points corresponding to individual cells. (k) Proportions of MEG3-positive and MEG3-negative cells in each CAF state. (l) Boxplot of m6A pathway activity scores across fibroblast subtypes. Boxplots include median, quartiles, and range, with individual points representing single cells. (m) Pseudotime trajectory illustrating the distribution of m6A pathway scores along the three CAF states. (n) Boxplot comparing m6A pathway activity scores among the three CAF states. Statistical significance was assessed using the two-sided Mann–Whitney test. *p < .05, **p < .01, ***p < .001.

Functional significance of the MEG3-expressing C4 subpopulation (MACAF) in tumor microenvironment interactions

To clarify the contribution of MEG3 to CAF activation processes, we conducted a detailed comparison of gene expression profiles between MEG3-positive and MEG3-negative cells. This revealed prominent activation of the epithelial-mesenchymal transition (EMT) pathway in MEG3-positive populations, most notably within fibroblasts. The pattern was corroborated by bulk RNA-seq data from multiple cancer types in the TCGA database. Pan-cancer analyses further confirmed a robust positive relationship between MEG3 transcript abundance and ssGSEA-computed EMT scores in both TCGA and ICGC datasets. Among fibroblast clusters, the C4 subtype exhibited the strongest EMT pathway enrichment **(Figure 3a)**. Moreover, MEG3 levels and EMT scores showed the highest correlation with the C4 subtype's ssGSEA enrichment score relative to all other fibroblast groups **(Figures 3b–3c)**. Regulatory network inference using SCENIC additionally highlighted activation of several EMT- and proliferation-related transcription factors (such as ZEB1, TWIST2, and SMAD5) specifically in MEG3-positive fibroblasts. Taken together, these data indicate that MEG3-positive fibroblasts—particularly those in the C4 cluster—are strongly linked to the induction of EMT programs in CAFs within the TME.

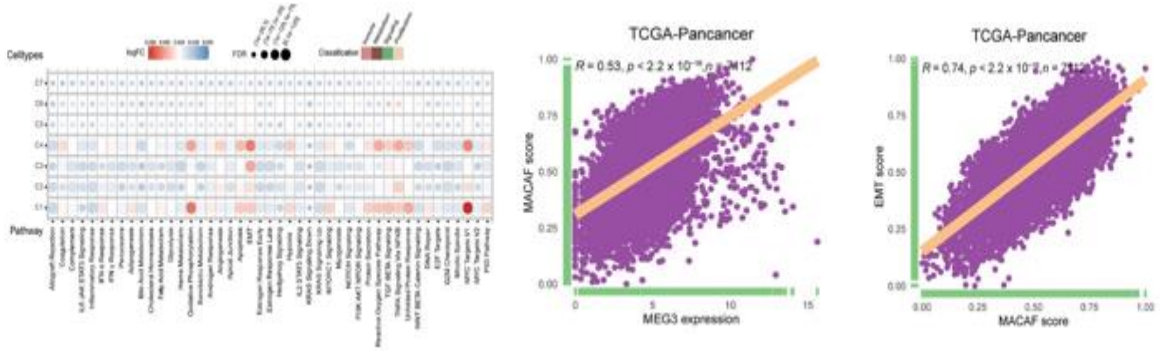

a) b) c)

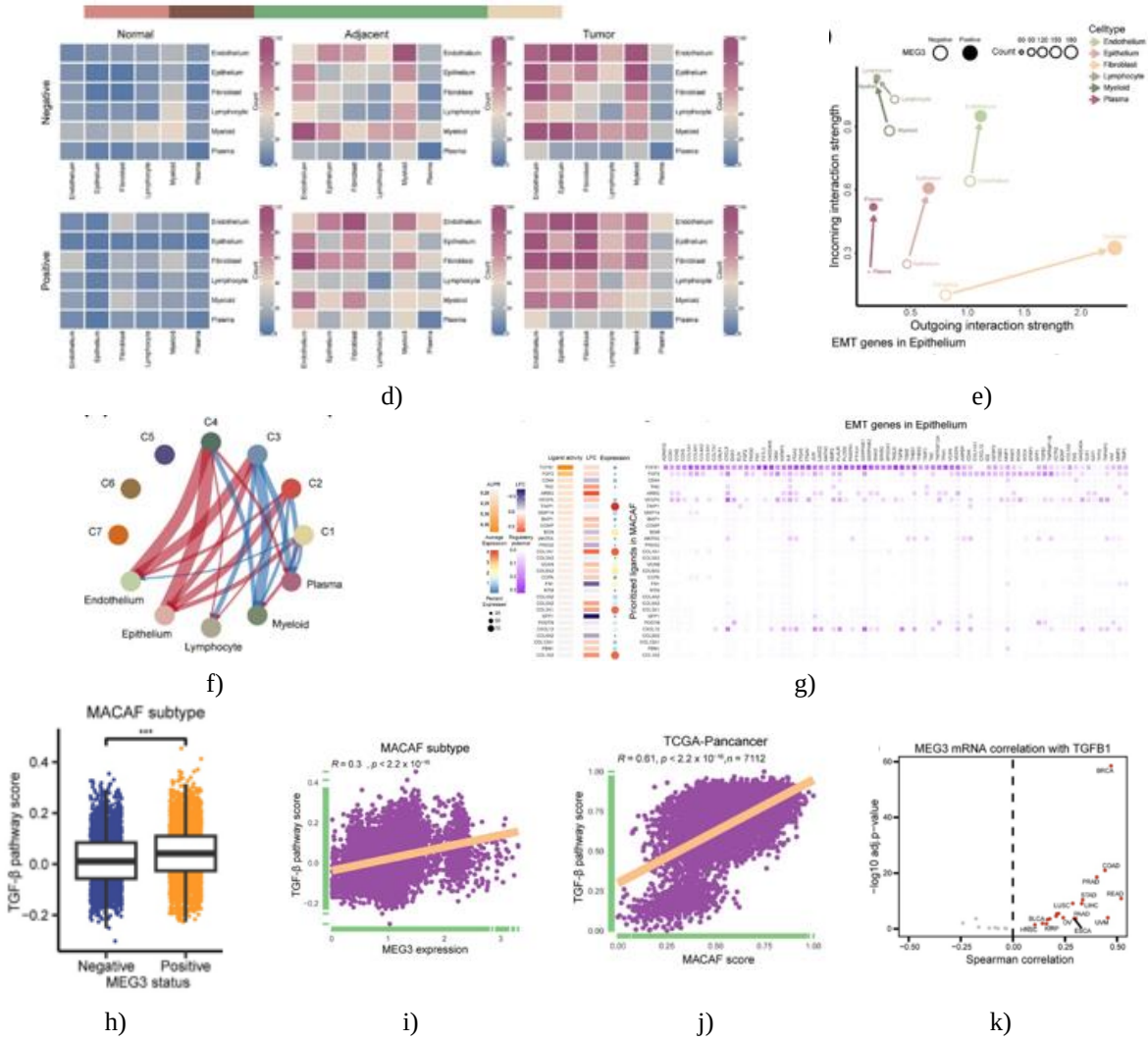

Figure 3. Detailed profiling of MEG3-positive versus MEG3-negative CAFs.
(a) Pathway enrichment differences between MEG3-positive and MEG3-negative cells across various CAF subtypes. (b) Spearman correlation analysis linking MACAF signature scores to MEG3 expression in the TCGA pan-cancer dataset. (c) Spearman correlation between MACAF subtype signature scores and EMT signature scores in the TCGA pan-cancer dataset. (d) Heatmap summarizing interaction frequencies among principal cell populations stratified by tissue type. (e) Bubble plots depicting shifts in signaling interaction strength for major cell types functioning as senders or receivers in MEG3-positive compared with MEG3-negative contexts. (f) Circle diagram illustrating variations in interaction counts among cell compartments between MEG3-positive and MEG3-negative groups. (g) Results from NicheNet ligand prediction for the EMT gene set, examining communication from the MACAF subpopulation to epithelial cells. Panels from left to right include: (1) Heatmap ranking candidate ligands produced by MACAF cells according to area under the precision-recall curve (AUPR) performance; (2) Heatmap of log2-fold changes for the leading ligands between MEG3-positive and MEG3-negative cells in the MACAF group; (3) Bubble plot showing relative expression of top ligands within the MACAF subpopulation; (4) Heatmap of predicted downstream targets in epithelial cells along with their regulatory interaction strengths, using MACAF as the source population. (h) Boxplot of TGF-β pathway activity scores in MEG3-positive versus MEG3-negative cells within the MACAF subtype. Boxplots indicate median, interquartile ranges, and extremes, with each dot representing an individual cell. (i) Spearman correlation of MEG3 expression with TGF-β pathway scores in the MACAF subpopulation. (j) Spearman correlation between MACAF subtype signature scores and TGF-β pathway activity across the TCGA pan-cancer cohort. (k) Volcano plot displaying per-cancer-type Spearman correlations between MEG3 and TGFB1 mRNA levels in TCGA. Red dots mark cancer types with significant positive associations (adjusted $p < .05$). Statistical testing was conducted with the Wilcoxon rank-sum test. *$p < .05$, **$p < .01$, ***$p < .001$.

To more thoroughly examine the potential functional contributions of MEG3-expressing cancer-associated fibroblasts (CAFs), cell-cell interaction analyses were undertaken between fibroblasts and other cellular components stratified by MEG3 expression levels. Overall, the quantity of CellphoneDB-inferred cell-cell interactions progressively increased from normal tissues through adjacent tissues to tumor samples. MEG3+ fibroblasts displayed a greater number of interactions with other cell populations than their MEG3− counterparts, most prominently in exchanges with epithelial cells and endothelial cells **(Figure 3d)**.

In agreement with these observations, CellChat-based evaluation of incoming and outgoing signals revealed a substantial strengthening of fibroblast-derived signaling activity within the MEG3+ population **(Figure 3e)**. Considering that endothelial and epithelial cells are capable of activating CAFs through the release of diverse cytokines (such as VEGF and PDGFD), the study next focused on identifying the ligand-receptor pairs specifically linked to MEG3-associated CAF activation. Differential examination of receptor-ligand interactions among fibroblast subtypes indicated that MEG3+ fibroblasts engaged in more extensive communication with both endothelial and epithelial cells compared with MEG3− fibroblasts, with this pattern being especially evident in the C4 subtype (MEG3+ adipogenic CAF, or MACAF) **(Figure 3f)**.

Owing to the robust associations identified between MEG3, epithelial cells, and epithelial-mesenchymal transition (EMT) processes **(Figures 3a, 3c and 3f)**, it was postulated that ligands originating from MACAFs might regulate EMT-related gene expression in nearby malignant epithelial cells. This hypothesis was tested through extended ligand-receptor modeling with NicheNet **(Figure 3g)**. Ligand activity scoring was initially applied to rank candidate ligands according to their capacity to predict changes across the EMT gene signature. TGFB1 stood out as the highest-ranked ligand, exhibiting the strongest predicted regulatory influence on EMT target genes in tumor epithelial cells **(Figure 3g)**. Moreover, TGF-β pathway activity scores were markedly elevated in MEG3+ MACAF cells relative to MEG3− cells **(Figure 3h)**, accompanied by a strong positive correlation within MACAF subpopulations **(Figure 3i)** as well as in the TCGA pan-cancer dataset **(Figure 3j)**.

The TGF-β pathway constitutes a key driver of CAF recruitment and infiltration, with its signaling closely linked to tumor cell invasive and migratory phenotypes [41]. Recent investigations have further demonstrated that TGF-β activation within CAFs can stimulate tumor cell migration and invasion [42, 43]. Collectively, these data imply that MEG3+ fibroblasts may interact with tumor epithelial cells via the TGF-β axis, thereby promoting EMT. Pan-cancer analyses additionally highlighted considerable heterogeneity in the strength of this crosstalk across tumor types, with particularly pronounced associations observed in BRCA, COAD, PRAD, and READ **(Figure 3k)**.

To functionally confirm whether interactions between MEG3+ fibroblasts and tumor epithelial cells augment EMT, stable MEG3-knockdown fibroblast lines were established via lentiviral transduction in patient-derived intestinal carcinoma fibroblasts (CAF1 and CAF2) and in the murine NIH3T3 fibroblast line **(Figures 4a–4c)**. Conditioned media were subsequently collected from both control and MEG3-knockdown CAF cultures and applied to human (HCT116, RKO) and murine (MC38, CT26) tumor cell lines. Transwell migration assays revealed that conditioned medium from control CAFs significantly boosted tumor cell motility, whereas MEG3 depletion in CAFs resulted in an even greater enhancement of migratory capacity **(Figures 4d–4m)**.

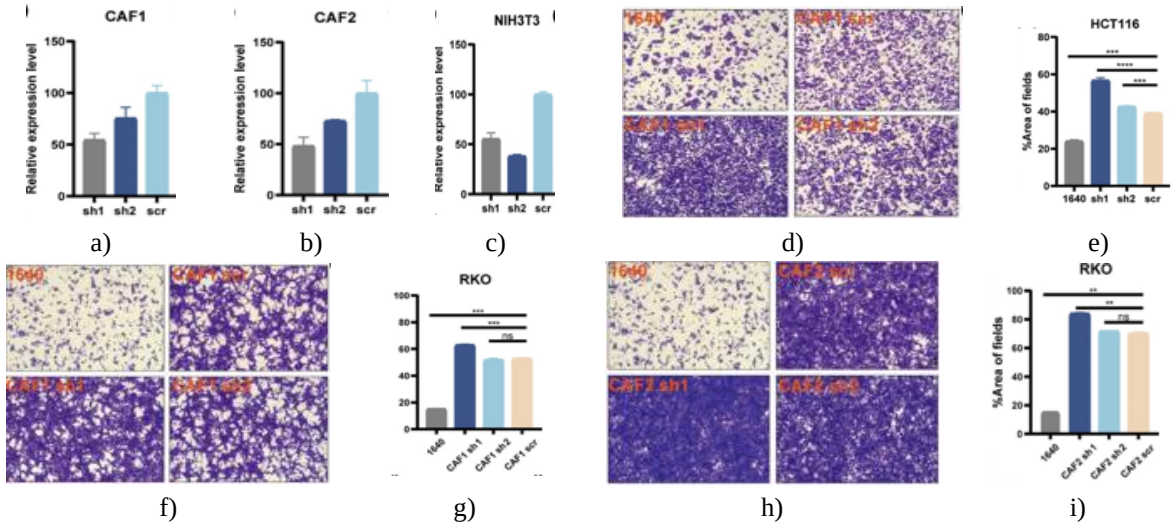

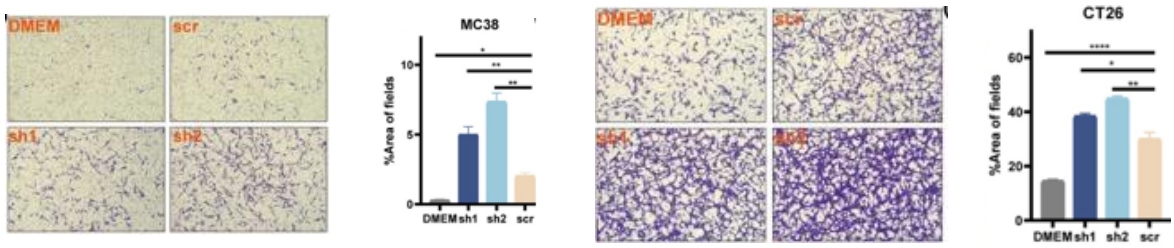

j) k) l) m)

Figure 4. MEG3 knockdown in CAFs enhances cancer cell migration.
Transwell migration assays were performed with HCT116, RKO, MC38, and CT26 cells exposed to conditioned medium from CAF1, CAF2, and NIH3T3 cells transfected with scrambled RNA (scr), shRNA1 (sh1), or shRNA2 (sh2). (a-c) Real-time quantitative PCR (qPCR) analysis of MEG3 expression levels in CAF1, CAF2, and NIH3T3 cells following transfection with scrambled RNA (scr), shRNA1 (sh1), or shRNA2 (sh2). (D-M) Representative images of migrated cells stained with 0.05% crystal violet are shown on the left (d, f, h, j, l) for each condition. Quantitative measurements of migrated cell area on the right (e, g, i, k, m) were obtained using ImageJ software. Statistical significance was assessed by the Wilcox test. *p < .05, **p < .01, ***p < .001.

Additionally, assessment of signaling pathway information flow within the MACAF subtype demonstrated enriched activity of several pathways—including PDGF, NOTCH, and SPP1—in MEG3+ cells compared with MEG3− cells, highlighting the distinctive role of this fibroblast subpopulation. Elevated PDGFRA expression was noted in MACAF cells, and the frequency of MEG3 positivity correlated strongly with PDGFRA positivity across fibroblast subtypes. Double-positive MEG3+PDGFRA+ cells were predominantly enriched in the C4 (MACAF) subtype. Furthermore, significant positive correlations between MEG3 and PDGFRA expression were detected at both bulk and single-cell transcriptomic levels, most prominently in the C4 MACAF population. In summary, these results support the involvement of MEG3 in tumor progression by modulating CAF interactions with other cell compartments through PDGFRA-mediated signaling.

Clinical utility of the MACAF score in guiding dasatinib therapy and immunotherapy

Since MEG3 functions as a long non-coding RNA and is therefore not readily amenable to direct pharmacological targeting, in silico compound screening was carried out among patients displaying elevated MACAF scores. Integration of data from two comprehensive drug sensitivity databases (CTRP and PRISM) identified Dasatinib as the single shared therapeutic candidate **(Figures 5a and 5b)**. As a potent PDGF receptor inhibitor, Dasatinib holds particular relevance in this context. Patients characterized by high MEG3 levels are expected to harbor greater infiltration of adipogenic CAFs along with elevated PDGF receptor expression, potentially conferring increased sensitivity to Dasatinib. Supporting this notion, previous work has established that Dasatinib treatment can promote the phenotypic conversion of CAFs back toward normal fibroblasts [44]. Thus, upregulated MEG3 expression in tumors may serve as an indicator of heightened PDGF receptor activity, thereby identifying patients who could benefit most from Dasatinib. In this manner, pharmacological inhibition of PDGFRA signaling with Dasatinib emerges as a viable strategy to reprogram the CAF phenotype in individuals with high MACAF scores.

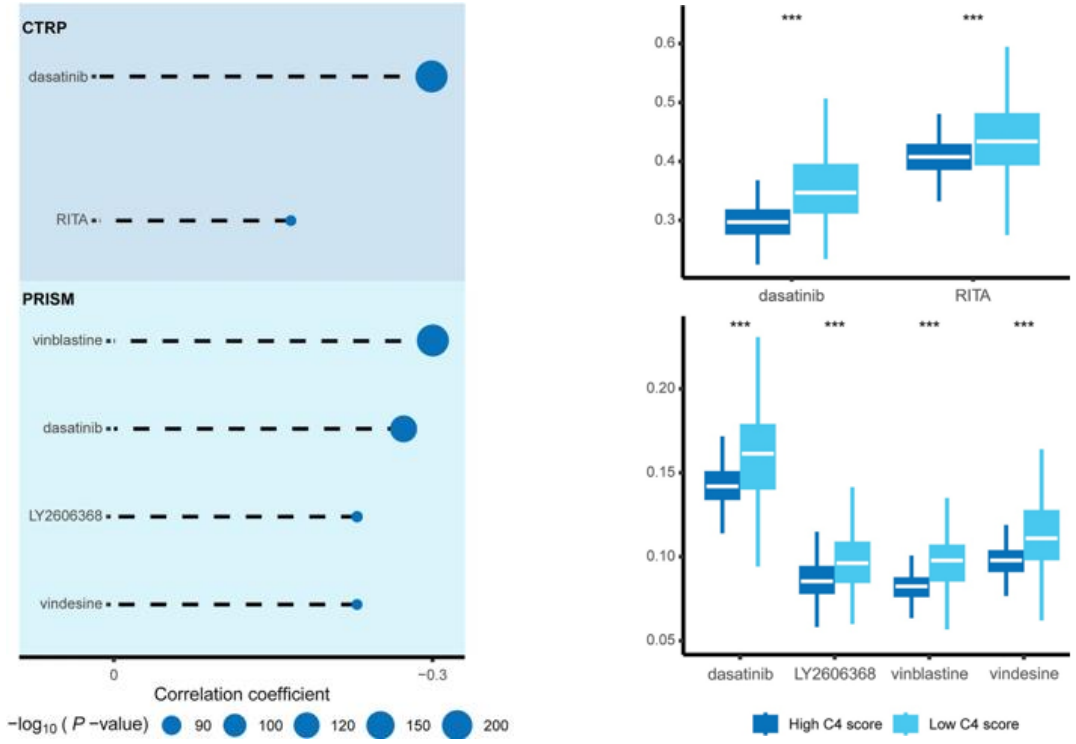

a) b)

Figure 5. Pharmacological targeting of the MACAF subtype as a therapeutic opportunity. (a) Spearman's correlation analysis of candidate agents from CTRP and PRISM databases, selected according to MACAF scores. (b) Differences in predicted AUC values for candidate compounds from CTRP and PRISM, stratified by MACAF scores. Statistical analysis was performed using the Wilcox test. *p < .05, **p < .01, ***p < .001.

Separately, adipogenic CAFs play a central role in reshaping lipid metabolism within the tumor milieu [45]. The resulting tumor microenvironment—marked by acidosis, hypoxia, glucose scarcity, and lipid overload—exerts profound immunosuppressive effects that can compromise the effectiveness of cancer immunotherapies [46, 47]. Because MEG3 enhances fibroblast communication with epithelial cells while diminishing interactions with lymphocytes **(Figure 3d)**, it was reasoned that the MACAF subpopulation might influence outcomes following immune checkpoint blockade (ICB) treatment. Examination of bulk RNA sequencing data from three independent immunotherapy cohorts revealed a consistent link between higher MACAF scores and inferior survival **(Figures 6a and 6b)**. In addition, patients with low MACAF scores demonstrated a significantly higher response rate to both anti-PD1 and anti-CTLA4 regimens compared with those possessing high MACAF scores **(Figure 6c)**.

Further analysis across TCGA datasets confirmed a statistically significant inverse relationship between MACAF scores and objective response rates (ORR) to anti-PD-1/PD-L1 therapy (p = 0.007) **(Figure 6d)** [48]. Recognizing that immunotherapy success depends critically on the immune composition of the tumor microenvironment, predictive algorithms such as TIDE [49] have been established to estimate pretreatment likelihood of response to immune checkpoint inhibitors. Application of TIDE to the TCGA pan-cancer cohort showed markedly higher Tumor Immune Dysfunction and Exclusion scores, as well as greater T-cell dysfunction and exclusion signatures, in patients with elevated MACAF scores relative to those with lower scores **(Figures 6e–6g)**. These observations point to diminished immunotherapy responsiveness in the high MACAF group. To better understand the immunological basis for these differences, the expression patterns of key immune-related molecules were profiled **(Figure 6h)**. Patients with high MACAF scores displayed reduced levels of important immune checkpoint ligands (e.g., TNF) and receptors (e.g., TIGIT, PDCD1, CTLA4, CD27, and LAG3), together with lower expression of HLA antigen-presentation genes. This transcriptional profile was accompanied by decreased copy number amplifications and increased deletions affecting these loci **(Figure 6h)**.

Overall, the MACAF score appears to represent a valuable biomarker for tailoring treatment selection, supporting the use of Dasatinib-targeted therapy in patients with high scores and favoring immune checkpoint inhibitor-based immunotherapy in those with low scores.

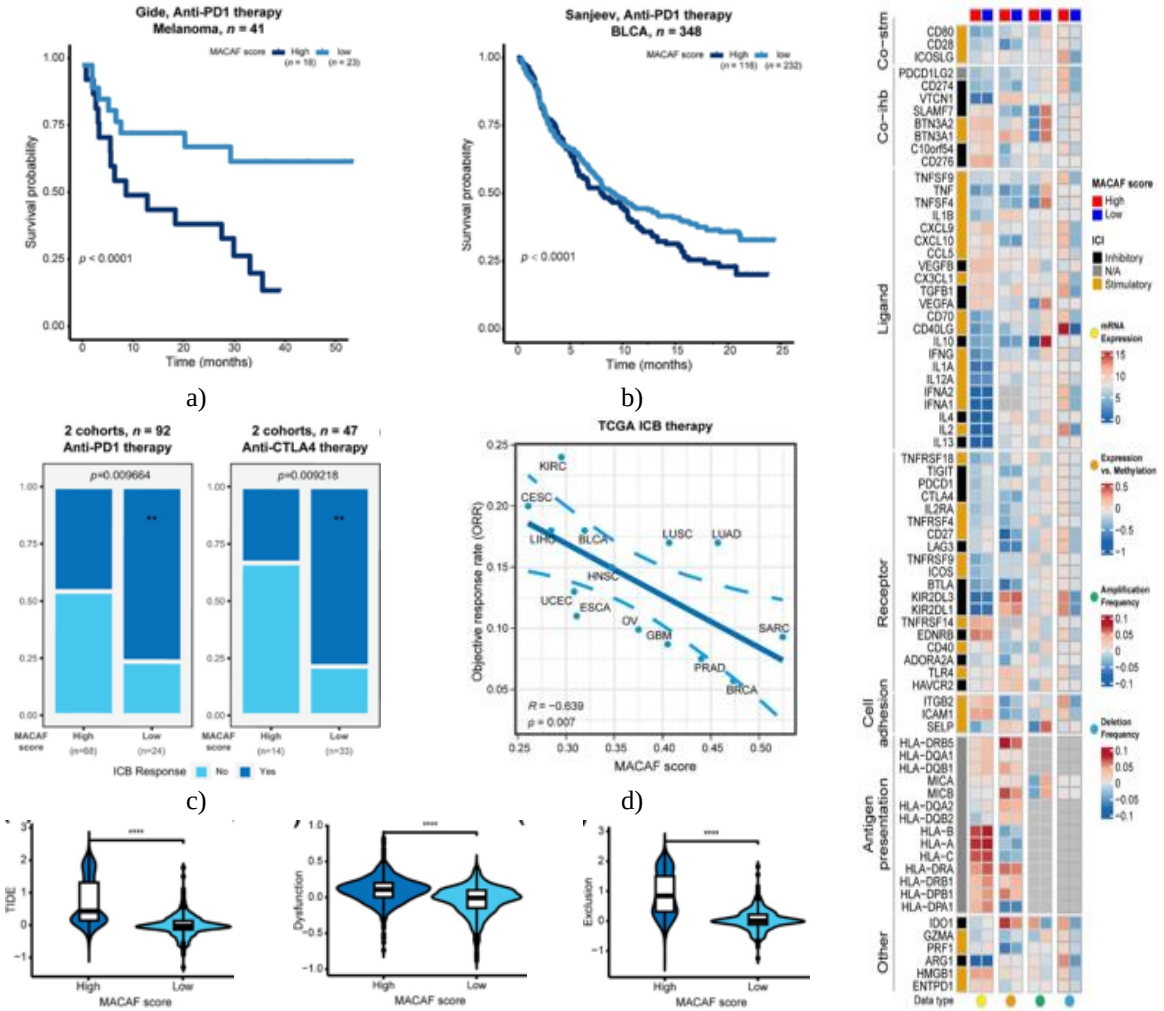

Figure 6. Relationship of MACAF score to immunotherapy efficacy.
(a-b) Kaplan–Meier overall survival curves demonstrating the prognostic relevance of MACAF scores in multiple immunotherapy cohorts. p-values were computed using the log-rank test. (c) Bar graph depicting the distribution of responders and non-responders among melanoma patients stratified according to MACAF scores. (d) Pearson correlation of MACAF scores with objective response rate (ORR) during Immune Checkpoint Blockade (ICB) treatment. Analysis included only non-zero values. (e-g) Outcomes of TIDE modeling in patients with high versus low MACAF scores. (h) Heatmap summarizing differences in immune regulatory factors between high and low MACAF score groups in melanoma. Panels display: median-normalized mRNA expression of selected modulators; Spearman correlations with methylation beta-values; amplification frequencies; and deletion frequencies of these modulators. Statistical tests included Fisher's exact test and Wilcox test. *p < .05, **p < .01, ***p < .001.

Elucidating the mechanisms underlying cancer-associated fibroblast (CAF) activation and their cellular origins within the tumor microenvironment continues to present a significant scientific challenge. Through systematic single-cell screening, MEG3 was identified as a long non-coding RNA that is selectively downregulated in fibroblasts derived from tumor tissues. Notably, although CAFs displayed a higher proportion of MEG3-positive cells, the average expression level of MEG3 within these MEG3+ CAFs remained relatively low—a pattern frequently observed with other tumor suppressor genes. This phenomenon may be explained by the induction of high tumor suppressor expression in aberrant cells under normal conditions, followed by its reduction once such cells are repaired or eliminated. In contrast, within tumor tissues, abnormal cells appear to tolerate modest levels of tumor suppressors, thereby evading corrective or eliminative processes. Consequently, a larger fraction of these abnormal cells express lower levels of the suppressor, underscoring their critical contribution to tumor progression. In the present context, this applies particularly to the MACAF subpopulation.

Prior research has largely attributed the reduced MEG3 expression observed in tumors to DNA methylation events [50-52]. However, such explanations fail to fully account for the increased prevalence of MEG3+ cells detected in single-cell profiling. Current knowledge regarding the dysregulated transcriptional regulation of MEG3 remains incomplete. The present analyses suggest that this characteristic feature in malignant tissues may arise from m6A-mediated post-transcriptional modifications. Although several investigations have described mutual regulatory interactions between MEG3 and m6A-related factors [53, 54], these studies were primarily conducted at the bulk transcriptome level in specific tumor types and centered on MEG3 function within epithelial cells. The current work reveals the progressive upregulation of MEG3 in fibroblasts during activation, followed by its suppression amid tumorigenesis. This perspective differs markedly from most existing literature, which has concentrated on genetic and epigenetic changes occurring directly within neoplastic cells. These results broaden current insights into the contributions of long non-coding RNAs to the biology of non-malignant stromal cells, especially fibroblasts, in the tumor microenvironment.

From a mechanistic standpoint, comprehensive transcriptional profiling was performed to compare MEG3+ and MEG3− CAF populations. While earlier studies had established connections between MEG3 and the epithelial-mesenchymal transition (EMT) pathway—typically indicating that MEG3 within tumor cells inhibits EMT and thereby restrains cancer advancement [55, 56]—this study provides the first pan-cancer single-cell demonstration of substantial differences in EMT activity between MEG3+ and MEG3− fibroblasts. The findings highlight a strong reliance on TGF-β signaling in mediating crosstalk between MEG3+ fibroblasts and tumor epithelial cells, which in turn promotes EMT. Functional validation was achieved by generating stable MEG3 knockdown fibroblast lines and assessing their conditioned medium effects on tumor cell motility, confirming that MEG3 depletion further augmented cancer cell migration. These observations reinforce the influential role of MEG3 in shaping tumor microenvironment interactions and raise intriguing questions about the opposing functional consequences of MEG3 expression in fibroblasts compared with tumor cells. Additionally, transcriptional upregulation of MEG3 was shown to drive increased PDGFRA receptor expression in CAFs, thereby strengthening their communicative interactions with endothelial and epithelial cells. Although previous reports have examined fibroblast-MEG3 relationships in non-malignant tissues [57-59] and explored general links between MEG3 and CAFs [60, 61], none have delineated its precise contributions in this setting. The present study characterizes the aberrant expression dynamics of MEG3 in CAFs and elucidates potential mechanisms through which it promotes CAF activation **(Figure 7)**. Overall, these data illustrate MEG3-driven fibroblast activation and associated cellular reprogramming within the tumor microenvironment, offering a novel conceptual framework for understanding lncRNA-mediated regulation of CAF biology.

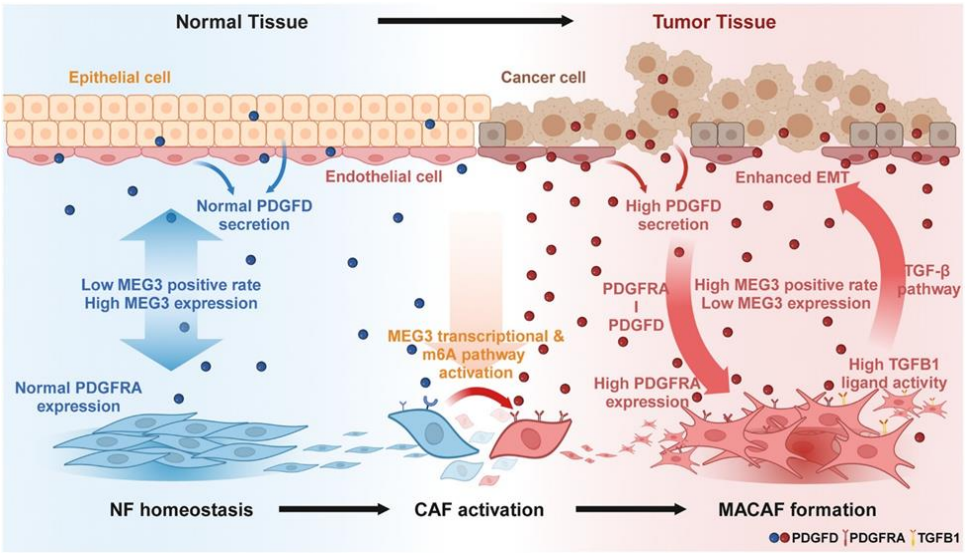

Figure 7. Schematic overview of MEG3 function in cancer-associated fibroblast (CAF) activation and its consequences for tumor advancement.

During tumor development, MEG3 transcription becomes activated in fibroblasts, engaging the m6A modification pathway. This leads to a notable divergence between the proportion of MEG3-positive cells and the overall

expression intensity of MEG3 within CAFs. The resulting transcriptional increase in MEG3 predominantly drives CAF activation, with adipogenic CAF-like cells (MACAF) representing the main affected subpopulation. Mechanistically, MACAF cells engage with neighboring tumor epithelial cells through TGF-β signaling, which stimulates the epithelial-mesenchymal transition (EMT) program and may thereby facilitate tumor invasion and progression. Reciprocally, signals from epithelial and endothelial cells further upregulate MEG3 in CAFs, largely by elevating PDGFRA expression in response to ligands such as PDGFD.

It was determined that MEG3 expression is most prominent within the MACAF subtype. Screening across two pharmacogenomic databases indicated that patients with elevated MACAF scores exhibit greater sensitivity to Dasatinib, aligning with the observed participation of MEG3 in PDGF-related signaling, given that Dasatinib functions as a established PDGF receptor inhibitor. Drawing upon earlier evidence, administration of Dasatinib to individuals with high MEG3 expression could potentially slow tumor advancement, representing a promising treatment option [44]. In addition, analyses centered on the C4 subtype demonstrated that MACAF scores effectively predict unfavorable clinical outcomes and diminished responses to immune checkpoint blockade (ICB) therapy. Considering the reduced immunotherapy benefit observed in high MACAF score patients, employing Dasatinib to target MACAF offers a practical alternative treatment approach for this population. In contrast, patients with low MACAF scores are more likely to achieve favorable outcomes with immune checkpoint inhibitors. Therefore, a MACAF-based scoring system provides useful guidance for stratifying patients and supports the development of individualized precision medicine approaches. Moreover, the strong link between MACAF activity and impaired immunotherapy efficacy underscores the critical contribution of this CAF subset to establishing an immunosuppressive tumor microenvironment. These discoveries deepen our comprehension of tumor microenvironment complexity and identify new opportunities for CAF-directed therapeutic interventions.

Although the present study provides important novel perspectives, several limitations should be noted. First, the majority of conclusions rely on bioinformatics approaches and lack extensive experimental confirmation. Consequently, many observations would benefit from additional validation through multi-omics integration. Second, while the potential involvement of MEG3 in CAF transformation and activation within tumors has been clarified, the precise molecular details governing this regulation require deeper investigation. The specific mechanisms linking MEG3 transcriptional activation to CAF stimulation and subsequent tumor promotion remain to be fully delineated. Finally, the translational relevance of MEG3, along with the clinical value of the MACAF score as both a prognostic marker and a guide for treatment decisions, demands rigorous validation in prospective clinical studies.

Conclusion

In summary, integrative analysis of single-cell RNA sequencing datasets across multiple cancer types has identified MEG3 as a prominent long non-coding RNA in cancer-associated fibroblasts. This investigation advances current knowledge regarding the regulatory mechanisms of CAF activation and intercellular communication mediated by MEG3, highlighting a distinctive transcriptional profile shaped by m6A-dependent post-transcriptional control. Notably, the MACAF score holds promise as a predictive biomarker to inform personalized treatment selection, directing the use of Dasatinib in patients with elevated MACAF scores and favoring immune checkpoint inhibitor (ICI)-based immunotherapy in those with lower scores.

Acknowledgments: None

Conflict of Interest: None

Financial Support: None

Ethics Statement: None

References

1. de Visser KE, Joyce JA. The evolving tumor microenvironment: From cancer initiation to metastatic outgrowth. Cancer Cell. 2023;41(3):374-92.

2. Luo H, Xia X, Huang LB, An H, Cao M, Kim GD, et al. Pan-cancer single-cell analysis reveals the heterogeneity and plasticity of cancer-associated fibroblasts in the tumor microenvironment. Nat Commun. 2022;13(1):6619.
3. Tang F, Li J, Qi L, Liu D, Bo Y, Qin S, et al. A pan-cancer single-cell transcriptional atlas of tumor-infiltrating myeloid cells. Cell. 2023;186(19):4235-51.
4. Zheng L, Qin S, Si W, Wang A, Xing B, Gao R, et al. Pan-cancer single-cell landscape of tumor-infiltrating T cells. Science. 2021;374(6574):abe6474.
5. Cheng S, Li Z, Gao R, Xing B, Gao Y, Yang Y, et al. A pan-cancer single-cell transcriptional atlas of tumor-infiltrating myeloid cells. Cell. 2021;184(3):792-809.
6. Yin D, Zhou T, Xia X, Han C, Liu Z, Li Q, et al. Single-cell analysis reveals the landscape of the tumor microenvironment in gastric cancer. MedComm–Oncology. 2023;2(3):e60.
7. Goenka A, Khan F, Verma B, Sinha P, Dmello CC, Jogalekar MP, et al. Tumor microenvironment signaling and therapeutics in cancer progression. Cancer Commun. 2023;43(5):525-61.
8. Wang R, Song S, Qin J, Yoshimura K, Peng F, Chu Y, et al. Evolution of immune and stromal cell states and spatial organization in the multistep progression of gastric cancer. Cancer Cell. 2023;41(8):1407-27.
9. Zhang Q, He Y, Luo N, Patel SJ, Han Y, Gao R, et al. Landscape and dynamics of single immune cells in hepatocellular carcinoma. Cell. 2019;179(4):829-45.
10. Zhang L, Yu X, Zheng L, Zhang Y, Li Y, Fang Q, et al. Lineage tracking reveals dynamic relationships of T cells in colorectal cancer. Nature. 2018;564(7735):268-72.
11. Yuan Z, Li Y, Zhang S, Wang X, Dou H, Yu X, et al. Single-cell transcriptomics reveals the cellular heterogeneity of the tumor microenvironment in gastric cancer. Mol Cancer. 2023;22(1):48.
12. Chhabra Y, Weeraratna AT. Fibroblasts in cancer: Unity in heterogeneity. Cell. 2023;186(8):1580-94.
13. Pitt JM, Marabelle A, Eggermont A, Soria JC, Kroemer G, Zitvogel L. Targeting the tumor microenvironment: Removing obstruction to anticancer immune responses and immunotherapy. Ann Oncol. 2016;27(8):1482-92.
14. Rimal R, Desai P, Daware R, Hosseinnejad A, Prakash J, Lammers T, et al. Cancer-associated fibroblasts: Origin, function, and therapeutic targeting. Adv Drug Deliv Rev. 2022;189:114504.
15. Lavie D, Ben-Shmuel A, Erez N, Scherz-Shouval R. The role of cancer-associated fibroblasts in cancer progression and therapy. Nat Cancer. 2022;3(7):793-807.
16. Mao X, Xu J, Wang W, Liang C, Hua J, Liu J, et al. Crosstalk between cancer-associated fibroblasts and immune cells in the tumor microenvironment: New findings and future perspectives. Mol Cancer. 2021;20(1):131.
17. Zhang H, Yue X, Chen Z, Liu C, Wu W, Zhang N, et al. Single-cell and spatial transcriptomics reveal the immune microenvironment of hepatocellular carcinoma. Mol Cancer. 2023;22(1):159.
18. Kotsiliti E. Single-cell and spatial transcriptomics in gastrointestinal cancers. Nat Rev Gastroenterol Hepatol. 2022;19(2):79-80.
19. Foster DS, Januszyk M, Delitto D, Yost KE, Griffin M, Guo J, et al. Multiomic analysis reveals conservation of cancer-associated fibroblast phenotypes across species and tissue of origin. Cancer Cell. 2022;40(11):1392-406.
20. Chen Y, Zhu S, Liu T, Zhang S, Lu J, Fan W, et al. Single-cell transcriptomics reveals the cellular heterogeneity of the tumor microenvironment in esophageal squamous cell carcinoma. Cancer Cell. 2023;41(5):903-18.
21. Wu F, Yang J, Liu J, Wang Y, Mu J, Zeng Q, et al. Signaling pathways in cancer-associated fibroblasts and targeted therapy. Signal Transduct Target Ther. 2021;6(1):218.
22. Liu Y, Xun Z, Ma K, Liang S, Li X, Zhou S, et al. Single-cell and spatial transcriptomics reveal the immune landscape of intrahepatic cholangiocarcinoma. J Hepatol. 2023;78(4):770-85.
23. Zhu GQ, Tang Z, Huang R, Qu WF, Fang Y, Yang R, et al. Single-cell transcriptomics reveals the cellular heterogeneity of the tumor microenvironment in hepatocellular carcinoma. Cell Discov. 2023;9(1):25.
24. Krishnamurty AT, Shyer JA, Thai M, Gandham V, Buechler MB, Yang YA, et al. LRRC15+ myofibroblasts dictate the stromal setpoint to suppress antitumor immunity. Nature. 2022;611(7934):148-54.
25. Ma C, Yang C, Peng A, Sun T, Ji X, Mi J, et al. Single-cell RNA sequencing reveals the landscape of the tumor microenvironment in gastric cancer. Mol Cancer. 2023;22(1):170.

26. Jenkins L, Jungwirth U, Avgustinova A, Iravani M, Mills A, Haider S, et al. Cancer-associated fibroblasts suppress CD8+ T-cell infiltration and function in breast cancer. Cancer Res. 2022;82(16):2904-17.
27. Grout JA, Sirven P, Leader AM, Maskey S, Hector E, Puisieux I, et al. Spatial positioning and matrix programs of cancer-associated fibroblasts promote T-cell exclusion in human lung tumors. Cancer Discov. 2022;12(11):2606-25.
28. Zhang Y, Liu Q, Liao Q. Tumor microenvironment and immunotherapy in pancreatic cancer. J Exp Clin Cancer Res. 2020;39(1):231.
29. Zhou L, Zhu Y, Sun D, Zhang Q. Cancer-associated fibroblasts: A new target for cancer immunotherapy. Int J Biol Sci. 2020;16(12):2094-105.
30. Zeng H, Hou Y, Zhou X, Lang L, Luo H, Sun Y, et al. Single-cell RNA sequencing reveals the heterogeneity of cancer-associated fibroblasts in gastric cancer. Theranostics. 2022;12(17):7351-67.
31. Zheng S, Zou Y, Tang Y, Yang A, Liang JY, Wu L, et al. Single-cell and spatial transcriptomics reveal the immune microenvironment of colorectal cancer. OncoImmunology. 2022;11(1):e2020984.
32. Liu T, Han C, Fang P, Ma Z, Wang X, Chen H, et al. Single-cell transcriptomics reveals the cellular heterogeneity of the tumor microenvironment in lung adenocarcinoma. J Hematol Oncol. 2022;15(1):141.
33. Qu X, Liu B, Wang L, Liu L, Zhao W, Liu C, et al. Targeting cancer-associated fibroblasts for cancer therapy. Drug Resist Updat. 2023;68:100936.
34. Ren J, Ding L, Zhang D, Shi G, Xu Q, Shen S, et al. Single-cell RNA sequencing reveals the landscape of the tumor microenvironment in pancreatic ductal adenocarcinoma. Theranostics. 2018;8(14):3932-45.
35. Lei Y, Meng Q, Hong F, Zhao M, Gao X. Cancer-associated fibroblasts in the tumor microenvironment of gastric cancer. Cancer Lett. 2023;569:216319.
36. Mondal T, Subhash S, Vaid R, Enroth S, Uday S, Reinius B, et al. MEG3 long noncoding RNA regulates the TGF-β pathway genes through formation of RNA–DNA triplex structures. Nat Commun. 2015;6:7743.
37. Zhou Y, Zhong Y, Wang Y, Zhang X, Batista DL, Gejman R, et al. Activation of p53 by MEG3 non-coding RNA. J Biol Chem. 2007;282(34):24731-42.
38. Wang A, Chen Y, Shi L, Li M, Li L, Wang S, et al. Long non-coding RNA MEG3 inhibits the proliferation and metastasis of gastric cancer cells through the PI3K/AKT signaling pathway. J Transl Med. 2022;20(1):288.
39. Lan Y, Liu B, Guo H. MEG3-mediated regulation of the tumor microenvironment in gastric cancer. Mol Ther Nucleic Acids. 2021;24:768-80.
40. Peng D, Fu M, Wang M, Wei Y, Wei X. Single-cell RNA sequencing reveals the cellular heterogeneity of the tumor microenvironment in gastric cancer. Mol Cancer. 2022;21(1):104.
41. Erdogan B, Webb DJ. Cancer-associated fibroblasts modulate growth factor signaling and extracellular matrix remodeling to regulate tumor metastasis. Biochem Soc Trans. 2017;45(1):229-36.
42. Ishimoto T, Miyake K, Nandi T, Yashiro M, Onishi N, Huang KK, et al. Activation of transforming growth factor beta 1 signaling in gastric cancer-associated fibroblasts increases their motility, via expression of rhomboid 5 homolog 2, and ability to induce invasiveness of gastric cancer cells. Gastroenterology. 2017;153(1):191-204.
43. Haubeiss S, Schmid JO, Mürdter TE, Sonnenberg M, Friedel G, van der Kuip H, et al. Dasatinib reverses cancer-associated fibroblasts induced resistance to chemotherapy in non-small cell lung cancer. Mol Cancer. 2010;9:168.
44. Li Z, Sun C, Qin Z. Metabolic reprogramming of cancer-associated fibroblasts and its effect on cancer cell behavior. Theranostics. 2021;11(17):8322-36.
45. Bian X, Liu R, Meng Y, Xing D, Xu D, Lu Z. Lipid metabolism and cancer-associated fibroblasts: A new perspective on tumor progression. J Exp Med. 2021;218(1):e20201606.
46. Goncalves AC, Richiardone E, Jorge J, Polonia B, Xavier CPR, Salaroglio IC, et al. Metabolic reprogramming and drug resistance in cancer-associated fibroblasts. Drug Resist Updat. 2021;59:100797.
47. Lee JS, Ruppin E. Metabolic dependencies in the tumor microenvironment. JAMA Oncol. 2019;5(11):1614-5.
48. Jiang P, Gu S, Pan D, Fu J, Sahu A, Hu X, et al. Signatures of T cell dysfunction and exclusion predict cancer immunotherapy response. Nat Med. 2018;24(10):1550-8.
49. He Y, Dan Y, Gao X, Huang L, Lv H, Chen J. Single-cell transcriptomics reveals the heterogeneity of the tumor microenvironment in gastric cancer. Am J Physiol Endocrinol Metab. 2021;320(3):E598-609.

50. Gao Y, Huang P, Zhang J. Single-cell RNA sequencing in cancer research. J Transl Med. 2017;15(1):268.
51. Sellers ZP, Bolkun L, Kloczko J, Wojtaszewska ML, Lewandowski K, Moniuszko M, et al. MEG3 as a tumor suppressor in gastric cancer. Clin Epigenet. 2019;11(1):50.
52. Li K, Gong Q, Xiang XD, Guo G, Liu J, Zhao L, et al. Long non-coding RNA MEG3 inhibits the proliferation and metastasis of gastric cancer cells through the PI3K/AKT signaling pathway. J Transl Med. 2023;21(1):382.
53. Wu J, Pang R, Li M, Chen B, Huang J, Zhu Y. The role of cancer-associated fibroblasts in gastric cancer. OncoTargets Ther. 2021;14:3745-56.
54. Yang Z, Bian E, Xu Y, Ji X, Tang F, Ma C, et al. Cancer-associated fibroblasts and their role in gastric cancer progression. OncoTargets Ther. 2020;13:989-99.
55. Li J, Jiang X, Li C, Liu Y, Kang P, Zhong X, et al. MEG3 and its role in tumor suppression. J Cell Physiol. 2019;234(12):22947-58.
56. Piccoli MT, Gupta SK, Viereck J, Foinquinos A, Samolovac S, Kramer FL, et al. MEG3 is a novel regulator of the tumor microenvironment. Circ Res. 2017;121(5):575-89.
57. Wang Y, Wang J, Wei LJ, Zhu DM, Zhang JS. Long non-coding RNA MEG3 inhibits the proliferation of gastric cancer cells through the PI3K/AKT signaling pathway. Biomed Pharmacother. 2017;87:548-55.
58. Dill TL, Carroll A, Pinheiro A, Gao J, Naya FJ. The role of MEG3 in the regulation of the tumor microenvironment. Development. 2021;148(8):dev194027.
59. Dadafarin S, Rodríguez TC, Carnazza MA, Tiwari RK, Moscatello A, Geliebter J. MEG3 and its role in cancer. Cells. 2022;11(20):3181.
60. Sun Y, Hao G, Zhuang M, Lv H, Liu C, Su K. Long non-coding RNA MEG3 inhibits the proliferation and metastasis of gastric cancer cells. Yonsei Med J. 2022;63(3):229-40.
61. Yang C, Huang X, Li Y, Chen J, Lv Y, Dai S. Single-cell and spatial transcriptomics in cancer research. Brief Bioinform. 2021;22(1):bbaa164.